Biointerface Research in Applied Chemistry
Open-Access Journal (ISSN: 2069-5837)

Article
Volume 13, Issue 2, 2023, 110
https://doi.org/10.33263/BRIAC132.110

Application to Differential Transform Method for MHD Fluid Flow and Heat Transfer

Pradyumna Kumar Pattnaik [1], Swarnalata Jena [2], Satyaranjan Mishra [2,*], Priya Mathur [1]

[1] Department of Mathematics, Odisha University of Technology and Research, Bhubaneswar- 751029, Odisha, India; papun_pattnaik@gmail.com (P.K.P.);
[2] Department of Mathematics, Centurion University of Technology and Management, Odisha, India; swarnalatajena83@gmail.com (S.J.);
[3] Department of Mathematics, Siksha 'O' Anusandhan Deemed to be University, Bhubaneswar, Odisha, 751030, India; satyaranjan_mshr@yahoo.co.in(S.R.M.);
[4] Department of Mathematics, Poornima Institute of Engineering & Technology Jaipur, Rajasthan 302022, India; drpriyamathur21@gmail.com (P.M.);
* Correspondence: styaranjan_mshr@yahoo.co.in (S.R.M.);

Scopus Author ID 57191609762
Received: 2.12.2021; Accepted: 3.01.2022; Published: 24.03.2022

Abstract: Present study reveals the flow of a classical non-Newtonian fluid based on the Williamson model through a vertical flat plate. The free convective flow is generated because of the effect of buoyancy relating to the temperature. In addition to that, the influence of thermal radiation and heat source/sink in conjunction with the dissipative heat enhances the efficiency of transport phenomenon within the bounding surface. Well-proposed similarity transformation is used to transform the governing equation into ordinary. However, due to the dissipation, the nonlinear coupled problems are complex. For the solution, a semi-analytical approach such as differential transformation method (DTM) in association with the Padé approximant method is used instead of traditional numerical technique. Pade-approximant is useful to get a non-iterative solution without imposing the missing boundary conditions. It is a simple and effective way to determine the solutions of complex nonlinear problems with assumed boundary conditions at infinity. The physical significance of all the contributing parameters distinguished the flow properties are achieved and accessible graphically. Moreover, the validation of the present methodology with the traditional numerical technique is obtained, showing an excellent correlation in particular cases.

Keywords: Williamson model; Free convection; thermal radiation; Heat transfer; DTM-Padé method

1. Introduction

Body forces on fluid create natural convection flow problems that are frequently come across in fluid engineering. Such natural convection problems may be taken as convection flow about a plane surface, kept along the direction of the force. One of the cases was analyzed by Schmidt and Beckmann [1], considering the convection of air through a vertical surface in the existence of the earth's gravitational field. The impact of the magnetic field upon an electro-conductive fluid affecting the natural convection is generally experienced in aerospace engineering, design of nuclear reactors, and so many engineering applications. The heat transport phenomena of an electro-conductive non-Newtonian liquid through the surface via the interaction of magnetic field is analyzed by Mishra *et al*. [2]. Considering the impact of reacting species and non-uniformity in heat sources, they found that the applied magnetic field

has no effect on velocity distribution, but it has an opposite effect on the concentration and temperature of the fluid. Mishra *et al*. [3] also studied the MHD free convection flow by taking doubly stratified micropolar fluid. The transport phenomena on the natural convective of MHD fluid within a permeable medium were analyzed by Pattnaik and Biswal [4]. Impose of the importance of thermal radiation; several research works were carried out in fluid engineering. Many authors worked on the effect of solutal transport and radiating properties on MHD natural convective within a permeable medium [5, 6]. They have analyzed the effect in the case of an exponentially accelerated plane surface. Zhou [7] has introduced the differential transformation method (DTM), which is proved to be one of the most practical and well-established techniques to handle the governing equations. Later on, this method was verified with the decomposition method by Ayaz [8] and the numerical method by Kurnaz and Oturanc [9] for solving a system of linear and nonlinear differential equations. Further, DTM is used by Yaghoobi, and Torabi [10] to solve nonlinear problems, and results were compared with VIM ("*variational iteration method*"), HPM ("*homotopy perturbation method*"), PM ("*perturbation method*") to verify its accuracy. It is proved that DTM is the most accurate method to obtain solutions to this type of problem. Recently, Sepasgozara *et al*. [11] used the DTM method to find out the momentum and heat transport phenomenon results for non-Newtonian fluid. They also find the validity of this method is in good accordance with the numerical method. DTM is also used by Usman *et al*. [12] to solve the problem of heat transfers in the case of nanofluid and compared the results with R-K method. It is found that both the methods are in good agreement with each other.

DTM method holds good for solving problems in the bounded region, but the result becomes erroneous in the case of the unbounded region. So this method is jointly used with Pade approximation [13, 14] to solve nonlinear ordinary differential equations on an infinite domain. Later on, DTM Pade approximation is used by so many authors to obtain error-free solutions to more complex problems. A relative study was made considering DTM-Pade approximation and further numerical methods in solving a complex problem like convective flow within a permeable medium through a slant plate [15]. DTM and DTM Pade approximation was compared in solving the temperature distribution of MHD flow from a horizontal plane surface [16]. In both cases, the excellence of the DTM Pade approximation is established. A complex flow pattern, i.e., momentum characteristics in MHD flow, was examined by Azimi *et al*. [17] using DTM-Pade, and the result was compared with that obtained from numerical analysis to prove the supremacy of DTM-Pade over numerical analysis. Further infinite boundary conditions were worked out by Peker *et al*. [18] using the DTM-Pade method. The result was matched with that obtained from ADM ("*Adomian decomposition method*") and VIM ("*variational iteration method*").

More correct solutions were obtained in the case of DTM-Pade. However, this technique is also used to establish the velocity pattern imposing magnetic field by Thiagarajan and Senthil Kumar [19]. More complicated problems like MHD flow through plane surface within a permeable medium are solved by Baag *et al*. [20] using both DTM combined with Pade and R-K, based on shooting to check the reliability of both methods. Later on, MHD Falkner-Skan flow of an electroconductive liquid through a permeable medium is investigated by Pattnaik *et al*. [21] using both DTM-Pade and Runge-Kutta fourth-order method. They established that solutions with higher accuracy are obtained in the case of DTM-Pade in solving nonlinear boundary layer problems.

In recent times some effective studies have been done by researchers [24-31]. Few latest methods are developed by different researchers to prepare the augmentation in the flow

phenomena. The literature review revealed that because of the several industrial as well as engineering applications, the role of radiative heat transport is vital in this investigation. Therefore, in response to earlier studies presented in [32-34], it is noteworthy to analyze the current topic. This paper will discuss the heat transfer of MHD fluid flow using DTM.

2. Analysis of the Problem and Formulation

Free convection of non-Newtonian magnetohydrodynamic Williamson liquid past a vertical plate embedding with the porous medium is considered in the present investigation. Influences of gravitational force caus by buoyancy are incorporated in the momentum profiles, and in addition to that, the heat source and the thermal radiation enhance the flow properties. The flow pattern is considered laminar along the x-direction, and a uniform transverse magnetic field is imposed along the normal direction (Figure 1).

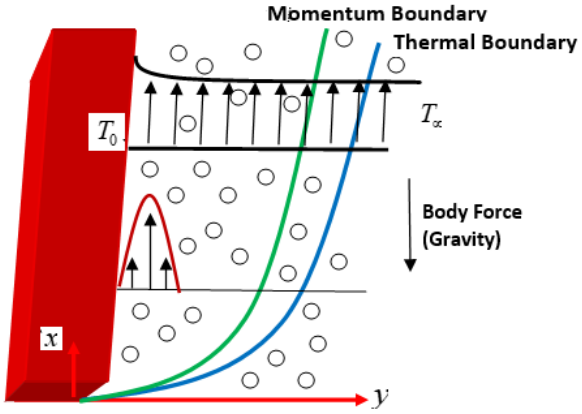

Figure 1. Flow geometry.

Assuming the aforementioned physical conditions the flow phenomena along with their boundary conditions are [1].

$$\frac{\partial u}{\partial x}+\frac{\partial v}{\partial y}=0 \tag{1}$$

$$u\frac{\partial u}{\partial x}+v\frac{\partial u}{\partial y}=\upsilon\frac{\partial^2 u}{\partial y^2}+\sqrt{2}\,\upsilon\gamma\frac{\partial u}{\partial y}\frac{\partial^2 u}{\partial y^2}-\left(\frac{\sigma B_0^2}{\rho}+\frac{\upsilon}{K_p^*}\right)u+g\beta\left(T-T_\infty\right) \tag{2}$$

$$u\frac{\partial T}{\partial x}+v\frac{\partial T}{\partial y}=\alpha\frac{\partial^2 T}{\partial y^2}+\frac{\mu}{\rho c_p}\left(\frac{\partial u}{\partial y}\right)^2+\frac{\sigma B_0^2}{\rho c_p}u^2+\frac{Q}{\rho c_p}\left(T-T_\infty\right)-\frac{1}{\rho c_p}\frac{\partial q_r}{\partial y} \tag{3}$$

$$\left.\begin{aligned}&u=v=0, T=T_0, \text{ at } y=0,\\&u\to 0, T\to T_\infty, \text{ as } y\to\infty.\end{aligned}\right\} \tag{4}$$

Using Roseland approximation for thermal radiation as

$$q_r=-\frac{4\sigma^*}{3\kappa}\frac{\partial T^4}{\partial y}.$$

where T^4, the temperature differences within the flow, can be expressed linearly and Taylor series expansion of T^4 at T_∞ with neglected higher-order terms which then yields $T^4=4T_\infty^4T-3T_\infty^4$ and $\frac{\partial q_r}{\partial y}=-\frac{16\sigma^*T_\infty^3}{3\kappa}\frac{\partial^2 T}{\partial y^2}$.

Eq. (3) then reduces to,

$$u\frac{\partial T}{\partial x}+v\frac{\partial T}{\partial y}=\left(\alpha+\frac{1}{\rho c_p}\frac{16\sigma^* T_\infty^3}{3\kappa}\right)\frac{\partial^2 T}{\partial y^2}+\frac{\mu}{\rho c_p}\left(\frac{\partial u}{\partial y}\right)^2+\frac{\sigma B_0^2}{\rho c_p}u^2+\frac{Q}{\rho c_p}\left(T-T_\infty\right) \tag{5}$$

Now introducing the similarity transformation

$$\eta=\sqrt{\frac{a}{\upsilon}}y,\psi=x\sqrt{a\upsilon}\,f(\eta),\theta(\eta)=\frac{T-T_\infty}{T_0-T_\infty},u=\frac{\partial\psi}{\partial y},v=-\frac{\partial\psi}{\partial x} \tag{6}$$

For which the continuity Eq.(1) is satisfied automatically.

Applying Eq.(6) into Eqs. (2) and (5) respectively, we obtain the following Eqs.(7) and (8),

$$\left(1+\lambda_2 f''\right)f'''(\eta)+f(\eta)f''(\eta)-\left(f'(\eta)\right)^2-\left(M+\frac{1}{Kp}\right)f'(\eta)+\lambda_1\theta=0 \tag{7}$$

$$\frac{1}{\Pr}\left(1+R\right)\theta''(\eta)+f(\eta)\theta'(\eta)+Ec\left(f''(\eta)\right)^2+M\,Ec\left(f'(\eta)\right)^2+S\,\theta(\eta)=0 \tag{8}$$

The transformed boundary conditions are as follows:

$$\begin{aligned}&f(\eta)=0,\ f'(\eta)=0,\theta(\eta)=1,\ \text{at}\ \ \eta=0,\\&f'(\eta)\to 0,\theta(\eta)\to 0,\qquad \text{as}\ \ \eta\to\infty.\end{aligned} \tag{9}$$

$$M=\frac{\sigma B_0^2}{\rho a},Kp=\frac{a}{\upsilon}K_p^*,Gr_x=\frac{g\beta\left(T_0-T_\infty\right)x^2}{\upsilon^2},\mathrm{Re}_x=\frac{ax^2}{\upsilon},\lambda_1=\frac{Gr_x}{\mathrm{Re}_x},$$

$$\lambda_2=\sqrt{\frac{2}{\upsilon}}\gamma a^{\frac{3}{2}}x,\Pr=\frac{\alpha}{\upsilon},R=\frac{16\sigma^* T_\infty^3}{3\rho c_p\alpha\kappa},Ec=\frac{\mu a^2x^2}{\rho c_p\upsilon\left(T_0-T_\infty\right)},S=\frac{Q}{a\rho c_p}.$$

3. Solution Technique

3.1. DTM approximations.

Zhou [7] in 1986 performed the study of differential transform. This is one of the processes to solve the set of differential equations using the semi-analytical technique. The basis of the method is Taylor series expansion, in which the equations are transformed into a recurrence relation in terms of polynomials to obtain a series solution. Firstly, the use of one-dimensional conversion of the problem to solve IVPs as well as BVPs for ordinary differential equations.

The differential transform of an analytical function $f(x)$ is defined as

$$F(k)=\frac{1}{k!}\left[\frac{d^k f(x)}{dx^k}\right]_{x=0} \tag{10}$$

where $F(k)$ is the transformed function.

However, the inverse transformation of $F(k)$ is defined as

$$f(x)=\sum_{k=0}^{\infty}F(k)(x-x_0)^k \tag{11}$$

By substituting equation (10) in (11) we get,

$$f(x)=\sum_{k=0}^{\infty}\frac{(x-x_0)^k}{k!}\left(\frac{d^k}{dx^k}f(x)\right)_{x=x_0} \tag{12}$$

However, the concept of these transformations is obtained from Taylor series expansion.

The fundamental DTM transformations are listed below in tabular form Table 1. But the DTM transformations we have used in our work are listed in Table 2. By taking the differential transforms of Eqs.7 and 8, respectively, we obtained Eqs. 13 and 14, respectively.

$$\left.\begin{aligned}&\frac{(k+3)!}{k!}F[k+3]+\sum_{r=0}^{k}(k-r+1)(k-r+2)F[r]F[k-r+2]+\lambda_1\Theta[k]\\&+\lambda_2\sum_{r=0}^{k}(r+1)(r+2)(k-r+1)(k-r+2)(k-r+3)F[r+2]F[k-r+3]\\&+\left(M+Kp^{-1}\right)(k+1)F[k+1]-\sum_{r=0}^{k}(r+1)(k-r+1)F[r+1]F[k-r+1]=0,\end{aligned}\right\} \tag{13}$$

$$\left.\begin{aligned}&\frac{1}{\Pr}(1+R)\frac{(k+2)!}{k!}\Theta[k+2]+Ec\sum_{r=0}^{k}(r+1)(r+2)(k-r+1)(k-r+2)F[r+2]F[k-r+2]\\&+\sum_{r=0}^{k}(k-r+1)F[r]\Theta[k-r+1]+M\,Ec\sum_{r=0}^{k}(r+1)(k-r+1)F[r+1]F[k-r+1]+S\,\Theta[k]=0.\end{aligned}\right\} \tag{14}$$

where $f(t)$ and $\theta(t)$ are the inverse differential transforms of $F(k)$ and $\Theta(k)$ respectively. Also, the transformed Boundary conditions are

$$F[0]=0,F[1]=0,F[2]=\frac{A}{2!},\Theta[0]=1,\Theta[1]=B. \tag{15}$$

Solving Eqns. (13 - 15) we can get the DTM solution as,

$$f(\eta)=\frac{A}{2}\eta^2-\frac{\lambda_1}{6}\eta^3+\frac{A_1}{24}\eta^4+\frac{A_2}{120}\eta^5+\frac{A_3}{720}\eta^6+\ldots \tag{16}$$

$$\theta(\eta)=1+B\eta-\frac{B_1}{2}\eta^2-\frac{B_2}{6}\eta^3+\frac{B_3}{24}\eta^4+\frac{B_4}{120}\eta^5-\frac{B_{12}}{120}\eta^6+\ldots \tag{17}$$

But to get accuracy in the solution of the boundary value problem of the present study, we have adopted Pade Approximant after applying DTM.

3.2. Pade Approximant.

A Pade approximation of $f(\eta)$ on $[a,b]$ can be expressed as a rational function that contains, $P_N(\eta)$ and $Q_M(\eta)$, two polynomials of degrees N and M, respectively [13]. Here, $[N/M]$ the ratio will denote the quotient. Moreover, to get better approximate results, the combined DTM and the diagonal Pade $[N/N]$ will be more powerful.

To accelerate the process of convergence of the obtained series, Baker and Morris [13] employed the so-called Pade approximant. Assuming a function $f(\eta)$ of the form,

$$f(\eta)=\sum_{i=0}^{\infty}c_i\eta^i \tag{18}$$

Here, $c_i, i = 0,1,2,\ldots$ are the constant coefficients and $f(\eta)$ is the associated function. $[L/M]$ Pade approximant is a rational fraction,

$$f(\eta) = \frac{a_0 + a_1\eta + a_2\eta^2 \ldots\ldots + a_L\eta^L}{b_0 + b_1\eta + b_2\eta^2 \ldots\ldots + b_M\eta^M} \tag{19}$$

It is to clarify that Eq.(19) has $L+1$ a numerator along with $M+1$ a denominator. There are numerator (unknowns) and independent denominator (unknowns) coefficients all total. Normally, $[L/M]$ it ought to fit the power series Eq.(18) through the orders $1, \eta, \eta^2, \ldots, \eta^{L+M}$. In the notation of formal power series

$$\sum_{i=0}^{\infty} c_i\eta^i = \frac{a_0 + a_1\eta + a_2\eta^2 + \ldots + a_L\eta^L}{b_0 + b_1\eta + b_2\eta^2 + \ldots + b_M\eta^M} + 0(\eta^{L+M}) \tag{20}$$

Here, arranging the coefficients of $\eta^{L+1}, \eta^{L+2}, \ldots, \eta^{L+M}$ we get,

$$\left.\begin{aligned} b_M c_{L-M+1} + b_{M-1}c_{L-M+2} + \ldots + b_0 c_{L+1} &= 0 \\ b_M c_{L-M+2} + b_{M-1}c_{L-M+3} + \ldots + b_0 c_{L+2} &= 0 \\ \ldots & \\ b_M c_L + b_{M-1}c_{L+1} + \ldots + b_0 c_{L+M} &= 0 \end{aligned}\right\} \tag{21}$$

For consistency, it is necessary to choose $c_i = 0$. As $b_0 = 1$, Eq. (21) consists of M unknown denominators to be determined.

$$\begin{pmatrix} c_{L-M+1} & c_{L-M+2}\ldots & c_{L+1} \\ c_{L-M+2} & c_{L-M+3}\ldots & c_{L+2} \\ c_L & c_{L+1}\ldots & c_{L+M} \end{pmatrix} \begin{pmatrix} b_M \\ b_{M-1} \\ \ldots \\ b_0 \end{pmatrix} = -\begin{pmatrix} c_{L+1} \\ c_{L+2} \\ \ldots \\ c_{L+M} \end{pmatrix} \tag{22}$$

The above expression shows that, b_i may be found. The coefficients contained in the numerator $a_0, a_1, \ldots\ldots a_L$ follow immediately from the equation (20) by equating the coefficients of $1, \eta, \eta^2, \ldots, \eta^{L+M}$ such as

$$a_0 = c_0, a_1 = c_1 + b_1c_0, a_2 = c_2 + b_1c_1 + b_2c_0, \ldots, a_L = c_L + \sum_{i=1}^{\min[L/M]} b_i c_{L-i} \tag{23}$$

Therefore, equations (20) and (23) evaluate the Pade numerator and denominator. Following, we have calculated diagonal Pade approximant of order [2/2] of $f'(\eta)$ and $g(\eta)$,

$$f'_{PADE}[2/2] = \frac{A\eta + \frac{(A^2A_2 + 4AA_1\lambda_1 - 3\lambda_1^3)}{2(3\lambda_1^2 - 2AA_1)}\eta^2}{1 + \frac{(AA_2 + 2A_1\lambda_1)}{2(3\lambda_1^2 - 2AA_1)}\eta - \frac{(4A\lambda_1^2 + 3A_2\lambda_1)}{12(2AA_1 - 3\lambda_1^2)}\eta^2} \tag{24}$$

$$\theta_{PADE}[2/2]=\frac{1+\left(B+\frac{BB_3-2B_1B_2}{2(3B_1^2+2BB_2)}\right)\eta+\frac{3B_1B_3-18B_1^3-24BB_1B_2+4B_2^2+6B^2B_3}{12(3B_1^2+2BB_2)}\eta^2}{1+\frac{BB_3-2B_1B_2}{2(3B_1^2+2BB_2)}\eta+\frac{4B_2^2+3B_3B_1}{12(3B_1^2+2BB_2)}\eta^2} \tag{25}$$

Solving Eqns.(24) and (25) for A and B as,

$$\lim_{\eta\to\infty} f'_{PADE[2/2]}(\eta)=0, \lim_{\eta\to\infty}\theta_{PADE[2/2]}(\eta)=0 \tag{26}$$

with some default values of all the parameters (varies in corresponding Figs.) as $M=1, Kp=0.5, \lambda_1=1, \lambda_2=1, R=0.1, \Pr=0.71, Ec=1, S=0.1$ we get $A=0.401892$ and $B=-0.427302$. So Eqns. (16) & (17) gives the desired solutions as:

$$f(\eta)=0.200946\eta^2-\frac{1}{6}\eta^3+0.158425\eta^4-0.00601047\eta^5+0.00532444\eta^6+\ldots \tag{27}$$

$$\theta(\eta)=1-0.427302\eta-0.461098\eta^2-0.246367\eta^3+0.521696\eta^4+0.123384\eta^5+0.100735\eta^6+\ldots \tag{28}$$

4. Results and Discussion

Free convective properties of an electrically conducting Williamson fluid past a vertical plate embedding within a permeable medium is considered in the present investigation. Inclusion of the dissipative heat caused by both the viscous and Joule affect the flow phenomena and also forms the system into coupled and nonlinear. Moreover, the energy equation is enhanced with the additional effects of heat source/sink and the thermal radiation. First, the governing equations are solved using the approximate analytical method employing DTM, and the Pade approximant technique obtains better accuracy. In particular cases, the current outcome validates with earlier established results numerically with a good agreement and shown in Figures. However, the comparison of the present computational result of longitudinal velocity, transverse velocity, and the temperature profiles with the numerical solution is obtained and displayed via graphs.

4.1. Validation of profiles.

In several cases, the present computational results validate with earlier numerical results and those are displayed in Figures 2-5. Figure 2 exhibits the comparison of longitudinal and transverse velocity profiles and the temperature profiles with numerical results in the particular case by withdrawing (write the parameters) and shows a good correlation for each distribution.

Figure 3 displays the comparison graph of stream function with respect to all the methodology applied, i.e., the DTM, DTM-Pade with numerical technique within a particular domain mentioned in the figure. It is observed that both the DTM and DTM-Pade agree well with each other, whereas the slight deviation of numerical results is remarked as the domain increases.

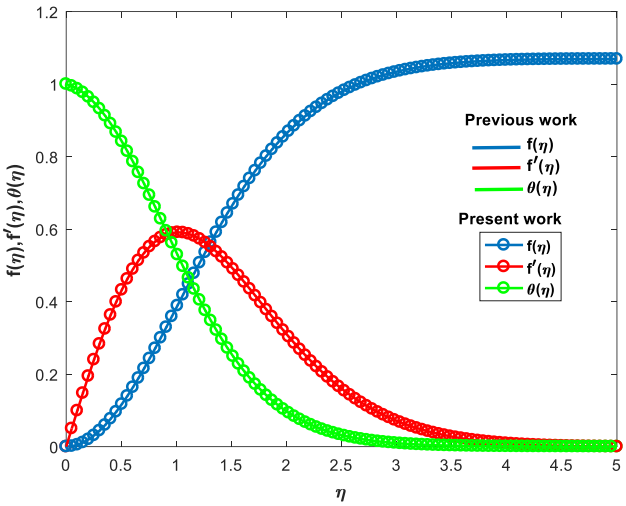

Figure 2. Validation of stream function, velocity, and temperature profile.

It is clear to conclude that higher-order Pade is useful to get the coincidence of the results. Figures 4 and 5 compare the velocity profile and the temperature profiles for the computational results by both DTM, DTM-Pade, and the earlier numerical method. The observation is similar to that of the results shown in Figure 3.

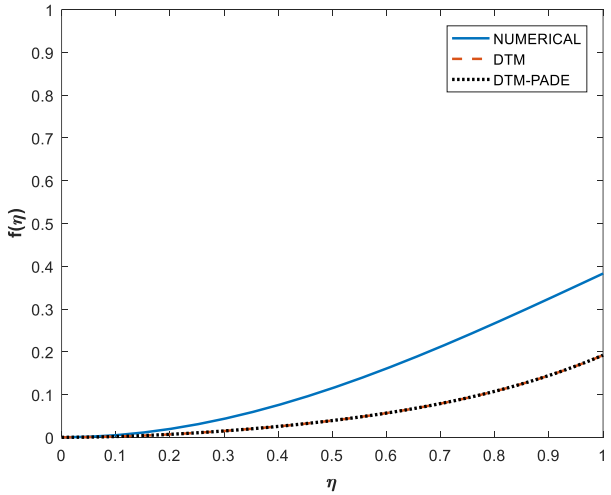

Figure 3. Comparison plot of stream function.

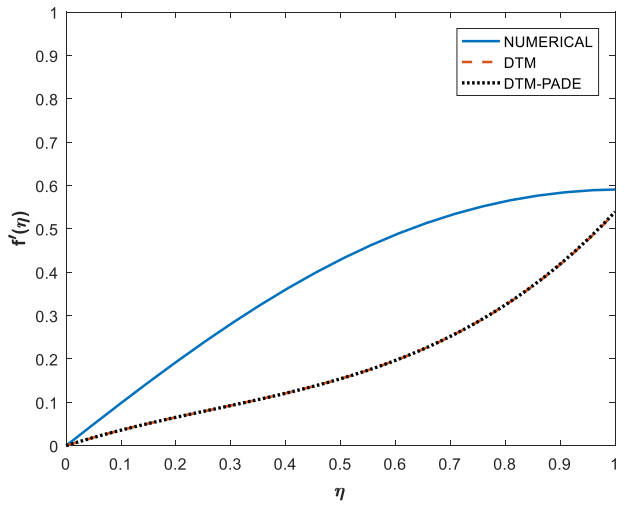

Figure 4. Comparison plot of the velocity profile.

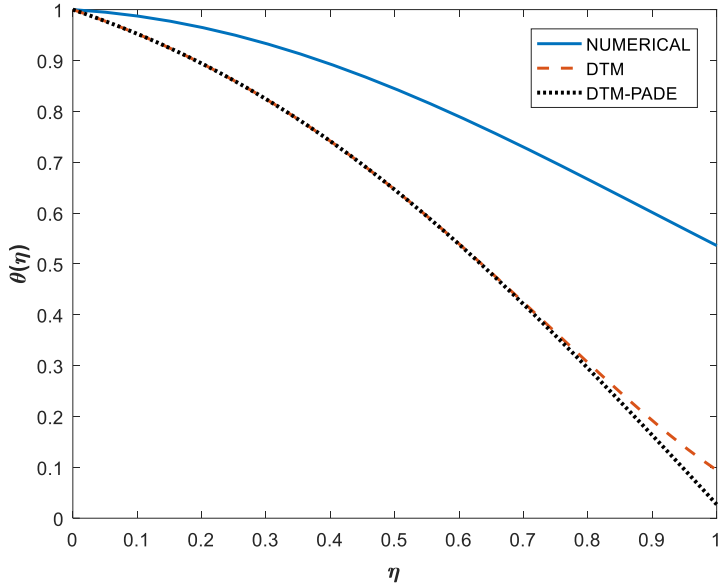

Figure 5. Comparison plot of the temperature profile.

4.2. Velocity profiles.

Figure 6 portrays the behavior of magnetic parameters in both the cases of the appearance/non-appearance of the porous matrix. From the mathematical point of view, the assumed value of Kp , $(Kp = 100)$ validates with the case of absence and Kp , $(Kp = 0.5)$ represents the presence of porous matrix. Inclusion of magnetic parameter exhibits an opposing force formed by the resistive force produced by "Lorentz force" that retards the flow domain. Therefore, the velocity profile retards the entire region of the boundary layer regardless of the occurrence/absence of the porous matrix. Similar to that, porosity is also a resistive force that retards the velocity profile as well. Figure 7 elaborates the influences of the thermal buoyancy parameter and the non-Newtonian parameter on the velocity distribution for the absence/presence of porous matrix. Pick in the flow velocity near the sheet is marked with an increasing value of the buoyancy parameter; however, the bounding surface thickness retards significantly.

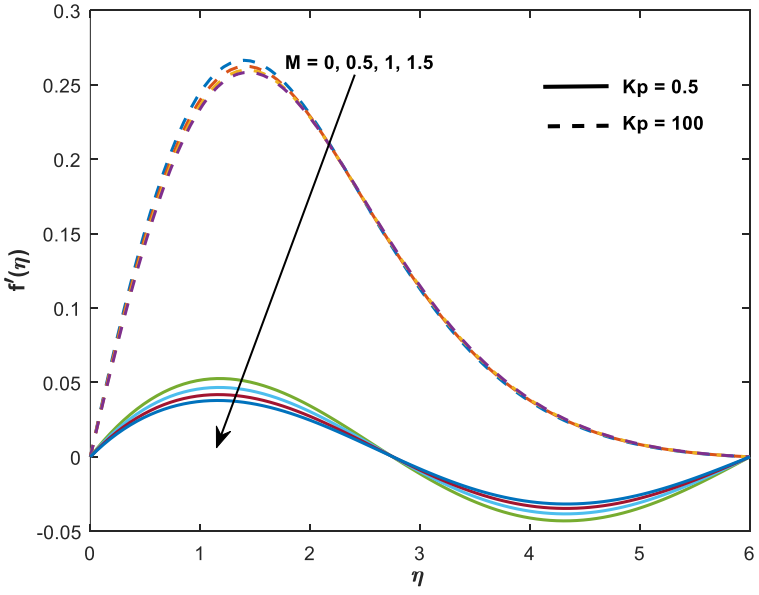

Figure 6. Influence of M and Kp on the velocity profile.

It is interesting to observe that, from the pick position, the profiles retards with opposite characteristics to that occurs near the plate to meet requisite conditions. An increase in porosity also retards the bounding surface thickness. It is also seen that the non-Newtonian parameter due to the flow characteristics of Williamson fluid retards the profiles near the sheet, and reverse effect is encountered from the point of inflection $\eta = 1.5$ to meet the appropriate boundary conditions.

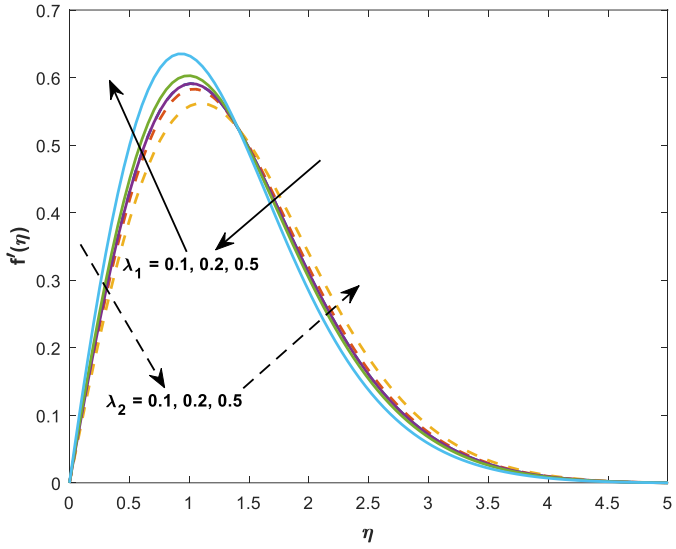

Figure 7. Influence of λ_1 and λ_2 on the velocity profile.

4.3. Temperature profiles.

The behavior of several contributing parameters on the temperature profiles of the non-Newtonian fluid is exhibited in Figures 8 and 9 for fixed values of other characterizing parameters. Figure 8 displays the effect of the Prandtl number on the fluid temperature in the presence of both magnetic and porosity. Is a usual phenomenon for the Prandtl number is that it decelerates the fluid temperature, resulting in the thermal boundary layer thickness retards. From the definition, it is clear that the Prandtl number increases mean there is a decrease in the thermal diffusivity. Therefore, the fluid temperature decreases. In the present case, the value of the Prandtl number is taken as 0.71 for the air at room temperature approximately $18^{o}C$ and the value 1 and 2 for gasses like ammonia (nearly 1.38). Hence, in the case of $Pr << 1$ the thermal diffusivity dominates to enhance the fluid temperature. Figure 9 exhibits the influences of magnetic parameter, Eckert number, thermal radiation, and heat source/sink parameter on the fluid temperature. It is seen that for the increase of all the contributing parameters, the temperature increases significantly. Inclusion of magnetic parameter that retards the velocity, the amount of stored energy boosts up to increase the thermal boundary layer. The appearance of the coupling parameter is due to the inclusion of dissipative heat energy in the energy equation. The increase of the Eckert number expresses the decrease in enthalpy difference, and that resulted in enhancing the profile. The emission of electromagnetic waves from all matter undergoes due to the radiative heat energy and causes an increase in fluid temperature of the non-Newtonian fluid. In advance, the heat source encourages the phenomenon, whereas the sink opposes it throughout the thermal boundary layer.

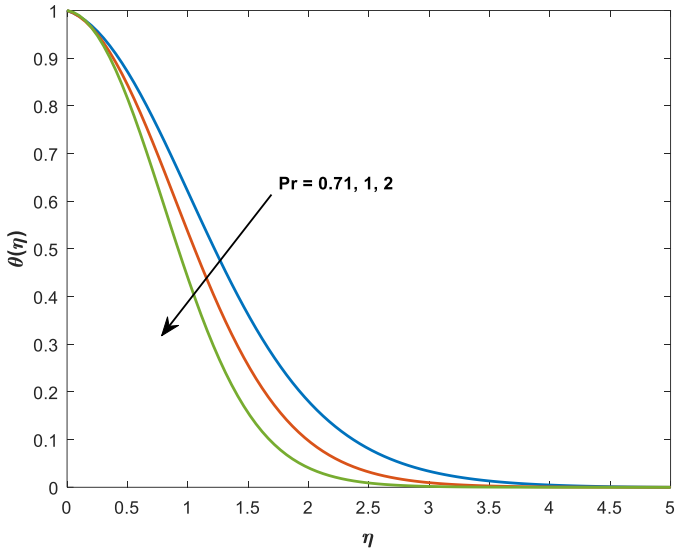

Figure 8. Influence of Pr on Temperature Profile.

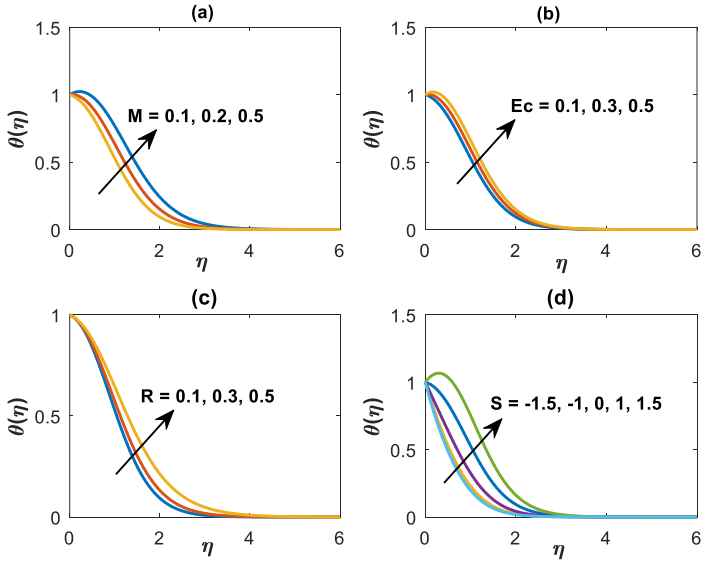

Figure 9. Influence of (a) M (b) Ec (c) R (d) S on temperature profile.

4.4. Engineering coefficients.

Finally, Figures 10-12 display the engineering coefficients such as shear rate and rate of heat transfer coefficients due to the variation of different parameters. The rate of shear stress versus magnetic parameter for the variation of thermal buoyancy parameter and the non-Newtonian parameter is exhibited in Figure 10. It displays that the rate increases as the magnetic strength increases and the increasing buoyancy also enhance it significantly. However, the non-Newtonian parameter has an opposing effect of lowering the shear stress rate. Figure 11 portrays the heat transfer rate versus the magnetic parameter with an increasing Prandtl number and the coupling parameter. It is seen that the Prandtl number is favorable to increase the rate, whereas retardation occurs due to the increase in the Eckert number. The rate of heat transfer with respect to the magnetic parameter for the improvement of heat source/sink and the radiation parameter is shown in Figure 12. It is clear that the source decreases the rate, whereas the sink increases. The increase of radiative heat energy boosts the rate significantly, whereas the increase of magnetic parameters ceases to decrease with a greater amount.

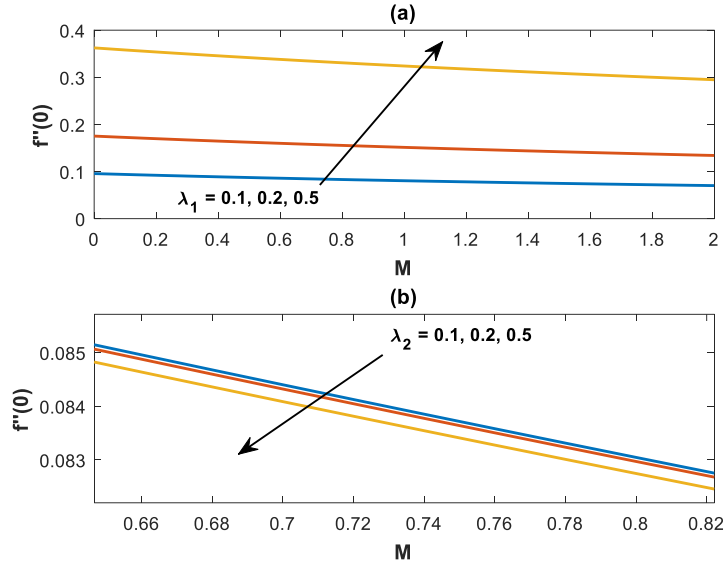

Figure 10. Variation of Skin Friction Coefficient with M, λ_1 and λ_2.

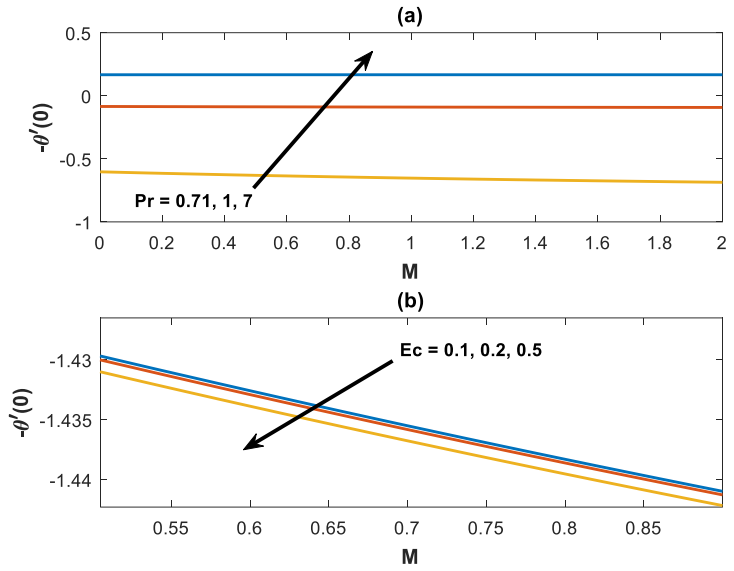

Figure 11. Variation of Nusselt number with M, Ec and Pr.

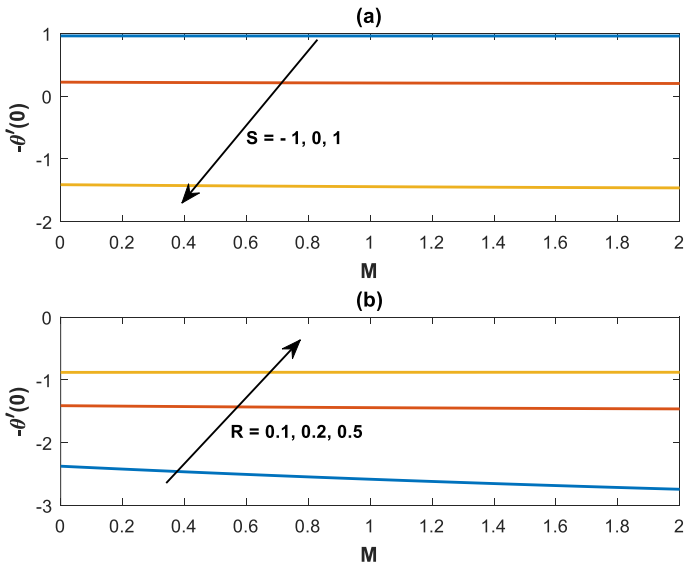

Figure 12. Variation of Nusselt Number with M, R and S.

Table 1. Standard Transformation rules of DTM.

Original Function	Transformed Function
$f(x)=u(x)\pm v(x)$	$F[k]=U[k]\pm V[k]$
$f(x)=\lambda u(x)$	$F[k]=\lambda U[k]$
$f(x)=x^m$	$F[k]=\begin{cases}1, & k=m\\ 0, & \text{otherwise}\end{cases}$
$f(x)=\dfrac{d^n u(x)}{dx^n}$	$F[k]=(k+1)(k+2)\ldots(k+n)U[k+n]$
$f(x)=u(x)v(x)$	$F[k]=\sum_{n=0}^{k}U[k]V[k-n]$
$f(x)=u'(x)v'(x)$	$F[k]=\sum_{n=0}^{k}(n+1)(k-n+1)U[k+1]V[k-n+1]$
$f(x)=u(x)v'(x)$	$F[k]=\sum_{n=0}^{k}(k-n+1)\,U[k]\,V[k-n+1]$

Table 2. Transformations used in the present problem.

Original Function	Transformed Function
$f(x)f'(x)$	$\sum_{r=0}^{k}(k-r+1)F(r)F(k-r+1)$
$f(x)f''(x)$	$\sum_{r=0}^{k}(k-r+1)(k-r+2)F(r)F(k-r+2)$
$f(x)f'''(x)$	$\sum_{r=0}^{k}(k-r+1)(k-r+2)(k-r+3)F(r)F(k-r+3)$
$f'(x)f''(x)$	$\sum_{r=0}^{k}(k-r+1)(k-r+2)(r+1)F(r+1)F(k-r+2)$
$f''(x)f'''(x)$	$\sum_{r=0}^{k}(k-r+1)(k-r+2)(k-r+3)(r+1)(r+2)F[r+1]F[k-r+3]$
$(f'(x))^2$	$\sum_{r=0}^{k}(k-r+1)(r+1)F(r+1)F(k-r+1)$
$f(x)g'(x)$	$\sum_{r=0}^{k}(k-r+1)F(r)G(k-r+1)$
$f(x)g''(x)$	$\sum_{r=0}^{k}(k-r+1)(k-r+2)F(r)G(k-r+2)$
$f'(x)g'(x)$	$\sum_{r=0}^{k}(k-r+1)^2F(k-r+1)G(k-r+1)$
$f''(x)g(x)$	$\sum_{r=0}^{k}(k-r+1)(k-r+2)G(r)F(k-r+2)$

5. Conclusions

An approximate analytical approach to the study of an electrically conducting Williamson non-Newtonian fluid past a vertical plate is presented in the current investigation. The inclusion of dissipative heat energy enhances the heat transfer properties significantly. Flow behavior and the heat transfer characteristics are observed for various contributing parameters and displayed via graphs. The physical properties of these parameters are deliberated in the discussion section. However, the main focus towards the significant results is appended as conclusive remarks. The current solution validates the earlier established results showing the proposed method's convergence criteria. The resistive force offered by the Lorentz force for the inclusion of magnetic field retards the velocity profiles. The stored energy boosts the fluid temperature due to the enhanced values of the Eckert number and dissipative heat

energy. The Williamson parameter is favorable to decrease the rate of shear stress coefficient. Heat source retards the heat transfer rate, whereas the impact becomes opposite for the sink parameter.

Funding

This research has received no external funding.

Acknowledgments

We are very much thankful to the learned reviewers for their valuable suggestions for improving the manuscript.

Conflicts of Interest

The authors have no conflict of interest.

References

1. Schmidt, E.; Beckmann, W. Das Temperatur-und Geschwindigkeitsfeld vor einer Wärme abgebenden senkrechten Platte bei natürlicher Konvektion. *Technische Mechanik und Thermodynamik* **1930**, *1*, 391-406.
2. Mishra, S.R.; Pattnaik, P.K.; Bhatti, M.M.; Abbas, T. Analysis of heat and mass transfer with MHD and chemical reaction effects on viscoelastic fluid over a stretching sheet. *Indian Journal of Physics* **2017**, *91*, 1219-1227, https://doi.org/10.1007/s12648-017-1022-2.
3. Mishra, S.R.; Pattnaik, P.K.; Dash, G.C. Effect of heat source and double stratification on MHD free convection in a micropolar fluid. *Alexandria Engineering Journal* **2015**, *54*, 681-689, https://doi.org/10.1016/j.aej.2015.04.010.
4. Pattnaik, P.; Biswal, T. Analytical Solution of MHD Free Convective Flow through Porous Media with Time Dependent Temperature and Concentration. *Walailak Journal of Science and Technology* **2015**, *12*, 749-762.
5. Pattnaik, J.R.; Dash, G.C.; Singh, S. Radiation and mass transfer effects on MHD flow through porous medium past an exponentially accelerated inclined plate with variable temperature. *Ain Shams Engineering Journal* **2017**, *8*, 67-75.
6. Mathur; P., Mishra; S.R., Free convective MHD flow over an exponentially stretching sheet with radiation, *Heat Transfer Asian Research*, **2019**, *48(7)*, 3371-3383**.**
7. Zhou, J.K. Differential transformation and its applications for electrical circuits. **1986**.
8. Ayaz, F. Solutions of the system of differential equations by differential transform method. *Applied Mathematics and Computation* **2004**, *147*, 547-567, https://doi.org/10.1016/S0096-3003(02)00794-4.
9. Kurnaz, A.; Oturanç, G. The differential transform approximation for the system of ordinary differential equations. *International Journal of Computer Mathematics* **2005**, *82*, 709-719, https://doi.org/10.1080/00207160512331329050.
10. Yaghoobi, H.; Torabi, M. The application of differential transformation method to nonlinear equations arising in heat transfer. *International Communications in Heat and Mass Transfer* **2011**, *38*, 815-820, https://doi.org/10.1016/j.icheatmasstransfer.2011.03.025.
11. Sepasgozar, S.; Faraji, M.; Valipour, P. Application of differential transformation method (DTM) for heat and mass transfer in a porous channel. *Propulsion and Power Research* **2017**, *6*, 41-48.
12. Usman, M.; Hamid, M.; Khan, U.; Mohyud Din, S.T.; Iqbal, M.A.; Wang, W. Differential transform method for unsteady nanofluid flow and heat transfer. *Alexandria Engineering Journal* **2018**, *57*, 1867-1875, https://doi.org/10.1016/j.aej.2017.03.052.
13. Baker Jr, G.A. Essentials of Padé Approximants, Ac. *Press, New York* **1975.**
14. Boyd, J.P. Padé approximant algorithm for solving nonlinear ordinary differential equation boundary value problems on an unbounded domain. *Computers in Physics* **1997**, *11*, 299-303, https://doi.org/10.1063/1.168606.

15. Rashidi, M.M.; Laraqi, N.; Sadri, S.M. A novel analytical solution of mixed convection about an inclined flat plate embedded in a porous medium using the DTM-Padé. *International Journal of Thermal Sciences* **2010**, *49*, 2405-2412, https://doi.org/10.1016/j.ijthermalsci.2010.07.005.
16. Rashidi, M.M.; Keimanesh, M. Using differential transform method and padé approximant for solving mhd flow in a laminar liquid film from a horizontal stretching surface. *Mathematical Problems in Engineering* **2010**, *2010*, https://doi.org/10.1155/2010/491319.
17. Azimi, M.; Ganji, D.D.; Abbassi, F. Study on MHD viscous flow over a stretching sheet using DTM-Pade'Technique. **2012,** https://doi.org/10.4236/mme.2012.24016.
18. Peker, H.A.; Karaoğlu, O.; Oturanç, G. The Differential Transformation Method and Pade Approximant for a Form of Blasius Equation. *Mathematical and Computational Applications* **2011**, *16*, https://doi.org/10.3390/MCA16020507.
19. Thiagarajan, M.; Senthilkumar, K. DTM-Pade approximants for MHD flow with suction/blowing. *Journal of Applied Fluid Mechanics* **2013**, *6*, 537-543.
20. Baag, S.; Acharya, M.R.; Dash, G.C. MHD Flow Analysis Using DTM-Pade'and Numerical Methods. *American Journal of Fluid Dynamics* **2014**, *4*, 6-15, https://doi.org/10.5923/j.ajfd.20140401.02.
21. Pattnaik; J. R., Dash; G. C., Ojha; K. L. MHD Falkner-skan flow through porous medium over permeable surface, *Modelling, Measurement and Control B* **2017,** *86*, 380-395, https://doi.org/10.18280/mmc_b.860205.
22. Seyyedi, S.M.; Dogonchi, A.S.; Hashemi-Tilehnoee, M.; Ganji, D.D.; Chamkha, A.J. Second law analysis of magneto-natural convection in a nanofluid filled wavy-hexagonal porous enclosure. *International Journal of Numerical Methods for Heat & Fluid Flow* **2020**, https://doi.org/10.1108/hff-11-2019-0845.
23. Molana, M.; Dogonchi, A.S.; Armaghani, T.; Chamkha, A.J.; Ganji, D.D.; Tlili, I. Investigation of Hydrothermal Behavior of Fe3O4-H2O Nanofluid Natural Convection in a Novel Shape of Porous Cavity Subjected to Magnetic Field Dependent (MFD) Viscosity. *Journal of Energy Storage* **2020**, *30*, 101395, https://doi.org/10.1016/j.est.2020.101395.
24. Jamshed, W.; Uma Devi S, S.; Goodarzi, M.; Prakash, M.; Sooppy Nisar, K.; Zakarya, M.; Abdel-Aty, A.-H. Evaluating the unsteady Casson nanofluid over a stretching sheet with solar thermal radiation: An optimal case study. *Case Studies in Thermal Engineering* **2021**, *26*, 101160, https://doi.org/10.1016/j.csite.2021.101160.
25. Naveen Kumar, R.; Punith Gowda, R.J.; Prasanna, G.D.; Prasannakumara, B.C.; Nisar, K.S.; Jamshed, W. Comprehensive study of thermophoretic diffusion deposition velocity effect on heat and mass transfer of ferromagnetic fluid flow along a stretching cylinder. *Proceedings of the Institution of Mechanical Engineers, Part E: Journal of Process Mechanical Engineering* **2021**, *235*, 1479-1489, https://doi.org/10.1177/09544089211005291.
26. Hussain, M; Ghaffar, A; Ali, A; Shahzad, A; Nisar, K.S.; Alharthi, M.R.; Jamshed, W. MHD thermal boundary layer flow of a Casson fluid over a penetrable stretching wedge in the existence of nonlinear radiation and convective boundary condition, *Alexandria Engineering Journal*, **2021**, *60(6)*, 5473-5483, https://doi.org/10.1016/j.aej.2021.03.042.
27. Shi, C.; Wang, M.; Yang, J.; Liu, W.; Liu, Z. Performance analysis and multi-objective optimization for tubes partially filled with gradient porous media. *Applied Thermal Engineering* **2021**, *188*, 116530, https://doi.org/10.1016/j.applthermaleng.2020.116530.
28. Mishra, S.R.; Mathur, P.; Ali, H.M. Analysis of homogeneous–heterogeneous reactions in a micropolar nanofluid past a nonlinear stretching surface: semi-analytical approach. *Journal of Thermal Analysis and Calorimetry* **2021**, *144*, 2247-2257, https://doi.org/10.1007/s10973-020-10414-6.
29. Pal, D.; Saha, P. Analysis of unsteady magnetohydrodynamic radiative thin liquid film flow, heat and mass transfer over a stretching sheet with variable viscosity and thermal conductivity. *International Journal for Computational Methods in Engineering Science and Mechanics* **2021**, *22*, 400-409, https://doi.org/10.1080/15502287.2021.1887406.
30. Hafeez, A.; Khan, M. Flow of Oldroyd-B fluid caused by a rotating disk featuring the Cattaneo-Christov theory with heat generation/absorption. *International Communications in Heat and Mass Transfer* **2021**, *123*, 105179, https://doi.org/10.1016/j.icheatmasstransfer.2021.105179.
31. Abbasi, A.; Mabood, F.; Farooq, W.; Khan, S.U. Radiation and joule heating effects on electroosmosis-modulated peristaltic flow of Prandtl nanofluid via tapered channel. *International Communications in Heat and Mass Transfer* **2021**, *123*, 105183, https://doi.org/10.1016/j.icheatmasstransfer.2021.105183.

32. Mathur, P.; Mishra, S.R. Free convective Poiseuille flow through porous medium between two infinite vertical plates in slip flow regime. *Pramana* **2020**, *94*, 69, https://doi.org/10.1007/s12043-020-1916-y.
33. Ejtemaee, P.; Khamehchi, E. Experimental investigation of rheological properties and formation damage of water-based drilling fluids in the presence of Al2O3, Fe3O4, and TiO2 nanoparticles. *Biointerface Research in Applied Chemistry* **2020**, *10*, 5886-5894, https://doi.org/10.33263/briac104.886894.
34. Boldyrev, A.; Ziganshin, M.; Mukhametzyanov, T.; Klimovitskii, A.; Lyadov, N.; Gerasimov, A. Formation of microspherical particles of albumin with model drug using spray drying process. *Biointerface Research in Applied Chemistry* **2019**, *9*, 4605-4611, https://doi.org/10.33263/briac96.605611.